Draft version September 29, 2016
Preprint typeset using LaTeX style emulateapj v. 12/16/11

# COSMOLOGICAL CONSTRAINTS FROM THE REDSHIFT DEPENDENCE OF THE GALAXY ANGULAR 2-POINT CORRELATION FUNCTION

Xiao-Dong Li,
School of Physics, Korea Institute for Advanced Study, 85 Heogiro, Dongdaemun-gu, Seoul 130-722, Korea

Cheng Cheng,
Kavli Institute for Theoretical Physics China, Institute of Theoretical Physics, Chinese Academy of Sciences, Zhong Guan Cun Street 55#, Beijing, 100190, P.R. China and
University of Chinese Academy of Sciences, P.R. China

Changbom Park,
School of Physics, Korea Institute for Advanced Study, 85 Heogiro, Dongdaemun-gu, Seoul 130-722, Korea

Hyunbae Park, Cristiano G. Sabiu,
Korea Astronomy and Space Science Institute, Daejeon 305-348, Korea

Juhan Kim[1],
Center for Advanced Computation, Korea Institute for Advanced Study, 85 Hoegi-ro, Dongdaemun-gu, Seoul 130-722, Korea and
School of Physics, Korea Institute for Advanced Study, 85 Heogiro, Dongdaemun-gu, Seoul 130-722, Korea

and

Sungwook E. Hong
School of Physics, Korea Institute for Advanced Study, 85 Heogiro, Dongdaemun-gu, Seoul 130-722, Korea
*Draft version September 29, 2016*

## ABSTRACT

We use the redshift dependence of the galaxy angular 2-point correlation function (2pCF) shape to constrain cosmological parameters. A wrongly adopted cosmology introduces redshift-dependent mis-scaling of the constructed galaxy distribution, leading to redshift-dependent rescaling in the measured angular 2pCF. We test our method on the HR4 mock galaxies having hundreds of millions of galaxies at redshifts 0, 0.5, 1, 1.5, 2. We find the redshift evolution of shape of angular 2pCF, as a function of scale, is sensitive to the adopted cosmological parameters. It is relatively insensitive to the gravitational growth of structure, the galaxy bias, and the redshift space distortion. Analyzing the 2pCF shape on scales $5h^{-1}$Mpc $\leq r_\perp \leq 40h^{-1}$Mpc, we derive tight constraints on $\Omega_m$ and $w$. The method could be applicable to future photometric surveys like DES, LSST to derive tight cosmological constraints. The work is a continue of our previous works (Li et al. 2014, 2015, 2016) as a strategy to constrain cosmological parameters based on some nearly redshift-invariant physical quantity; they are all powerful in constrain cosmology and have a lot of merits, e.g., are less affected by the systematic effects introduced by non-linear clustering or RSD, does not require accurate modeling of galaxy clustering, and are applicable on relative small clustering scales.

*Keywords:* large-scale structure of Universe — dark energy — cosmological parameters

## 1. INTRODUCTION

The discovery of cosmic acceleration (Riess et al. 1998; Perlmutter et al. 1999) implies the existence of a "dark energy" component in the Universe or the breakdown of Einstein's gravity theory on cosmological scales. The theoretical explanation and observational probe of cosmic acceleration has attracted tremendous effort in the last two decades and are still far from well understood or accurately measured (Weinberg 1989; Li et al. 2011; Weinberg et al. 2013).

In an effort to probe the cosmic expansion history the large scale structure (LSS) surveys enable measurements of two geometrical quantities, the angular diameter distance $D_A$ and the Hubble factor, $H$. If they were precisely measured as a function of redshift, tight constraints can be placed on cosmological parameters, e.g. the matter density $\Omega_m$ and the equation of state (EoS) of dark energy $w$.

As one geometrical effect of cosmological parameters on LSS, when an incorrect cosmological model is assumed for the coordinate transformation from redshift space to comoving space, geometric distortions are produced in the constructed galaxy distribution. These distortion include the "volume effect" which is the mis-scaling of the size of structures, and the Alcock-Paczynski (AP) effect, the shape distortion induced by the fact that distances along and perpendicular to the line of sight are fundamentally different.

Various statistically methods has been proposed to measure these effects. The AP effect has been proposed to measure through the clustering of galaxies (Ballinger Peacock & Heavens 1996; Matsubara & Suto 1996) which has been applied to a series of LSS surveys (Outram et

[1] Corresponding Author: kjhan@kias.re.kr

al. 2004; Blake et al. 2011; Chuang & Wang 2012; Reid et al. 2012; Beutler et al. 2013; Linder et al. 2014; Song et al. 2014; Jeong et al. 2014; Sutter et al. 2014; López-Corredoira 2014; Alam et al. 2016; Beutler et al. 2016; Sanchez et al. 2016), the alternative approaches using the symmetry properties of galaxy pairs (Marinoni & Buzzi 2010; Jennings et al. 2011; **?**) and cosmic voids (Ryden 1995; Lavaux & Wandelt 2012; Sutter et al. 2014; Mao et al. 2016). Methods proposed able to probe the volume effect include the number counting of galaxy clusters (Press & Shechter 1974; Viana & Liddle 1996) and topology (Park & Kim 2010), the BAO scale (Eisenstein et al. 1998; Blake & Glazebrook 2003; Seo & Eisenstein 2003), and the shape of 2pCF and power spectrum (Sáchez et al. 2006; Sánchez et al. 2009).

In Li et al. (2014, 2015, 2016) we developed a novel strategy to probe $D_A$ and $H$ from LSS data. We found fact that the AP or volume effect in general introduces a geometric distortion significantly evolves with redshift; this phenomenon can be utilized to distinguish the the from the other effects such as the redshift space distortion (RSD). The radial distances of galaxies are inferred from the measured redshifts which are distorted by the peculiar motion of galaxies, leading to apparent distortion in the redshift space galaxy distribution (Jackson 1972; Kaiser 1987; Ballinger Peacock & Heavens 1996). It is the major systematic effects limiting our ability to probe the geometry of LSS from galaxy distribution. We found its influence is significantly reduced in case of studying the redshift dependence of the distortion.

Li et al. (2014) attempted to use the *galaxy density gradient field* to characterize the redshift evolution of the LSS distortion. We tested the idea on Horizon Run 3 (HR3) N-body simulations (Kim et al. 2011), showing the redshift evolution of the statistical property of the gradient field can be used to infer unbiased constraints cosmological parameters and is insensitive to RSD. The same topic was revisited in Li et al. (2015), using the statistical tool of *galaxy two-point correlation function* (2pCF) as a function of angle, $\xi(\mu)$, where $\mu \equiv \cos\theta$ and $\theta$ is the direction between the connection of the galaxy pairs and the direction. When incorrect cosmological parameters are adopted, the shape of $\xi(\mu)$ is altered due to the anisotropic shape of the LSS (the AP effect), and the amplitude is shifted due to the change in the size of comoving volume; both effects have significant redshift dependence. The RSD effect, although *very significantly* distorts $\xi(\mu)$, exhibits less redshift evolution. The method was applied to BOSS DR12 galaxies (Li et al. 2016) to probe the redshift dependent of the AP effect, and we come up with tight cosmological constraints comparable to the mainstream probes of SNIa, BAO, CMB and so on.

In this paper we continue our exploration of our strategy and presented a new method using the redshift of the shape of *galaxy angular 2pCF* as a function of radial scale, $\omega(r_\perp)$, to constrain cosmology. A wrongly adopted cosmology result in *redshift-dependent mis-scaling* of the galaxy distribution, which leads to redshift-evolution of the shape of $\omega(r_\perp)$. The signal is sensitive to the cosmological parameters and relatively insensitive to the other effects such as the gravitational growth of structure, the galaxy bias, and the RSD effect. We apply our method to the HR4 mock galaxies having hundreds of million galaxies at redshfits 0-2 and develop the statistical procedure to constrain cosmological parameters.

The outline of this paper proceeds as follows. In §2 we briefly review the nature and consequences of the LSS geometric distortion when performing coordinate transforms in a cosmological context. In §3 we describe the N-body mock galaxies used to test our method. The methodology is presented in §4. We conclude in §5.

## 2. VOLUME EFFECT IN A NUTSHELL

In this section we briefly introduce the scaling effect caused by wrongly assumed cosmological parameters. A more detailed description has been provided in Li et al. (2014, 2015, 2016).

Suppose that we are probing the size of some objects in the Universe. We measure its redshift span $\Delta z$ and angular size $\Delta\theta$, then compute its sizes in the radial and transverse directions using the following formulas

$$\Delta r_\parallel = \frac{c}{H(z)}\Delta z, \quad \Delta r_\perp = (1+z)D_A(z)\Delta\theta, \tag{1}$$

where $H$ is the Hubble parameter and $D_A$ is the angular diameter distance. In the particular case of a flat universe composed by a cold dark matter component and a constant EoS dark energy component, they take the forms of

$$H(z) = H_0\sqrt{\Omega_m a^{-3} + (1-\Omega_m)a^{-3(1+w)}},$$
$$D_A(z) = \frac{1}{1+z}r(z) = \frac{1}{1+z}\int_0^z \frac{dz'}{H(z')}, \tag{2}$$

where $a = 1/(1+z)$ is the cosmic scale factor, $H_0$ is the present value of Hubble parameter and $r(z)$ is the comoving distance.

In case wrong values of $\Omega_m$ and $w$ are adopted, the inferred $\Delta r_\parallel$ and $\Delta r_\perp$ are wrong, resulting in wrong estimations of the object's shape (AP effect) and size (volume effect). These effects and their cosmological consequences have been studied in Li et al. (2014, 2015, 2016).

In this paper we focus on the mis-estimation of the angular size $\Delta r_\perp$. The ratio of mis-estimation is

$$\alpha_\perp \equiv \frac{\Delta r_{\perp,\rm wrong}}{\Delta r_{\perp,\rm true}} = \frac{D_{A,\rm wrong}}{D_{A,\rm true}}, \tag{3}$$

where "true" and "wrong" denote the values in the true cosmology and wrongly assumed cosmologies, respectively.

An illustration is provided in the left panels of Figure 1. Suppose that the true cosmology is a flat ΛCDM with present matter ratio $\Omega_m = 0.26$ and standard dark energy EoS $w = -1$. If we were to distribute a series of perfect squares at distances ranging from 500 Mpc/h to 3 000 Mpc/h, and an observer located at the origin were to measure their redshifts and infer the sizes of the squares using the distance-redshift relations of four incorrect cosmologies

$$\text{(i)}.\ \Omega_m = 0.40,\ w = -1.0,$$
$$\text{(ii)}.\ \Omega_m = 0.15,\ w = -1.0,$$
$$\text{(iii)}.\ \Omega_m = 0.26,\ w = -0.5,$$
$$\text{(iv)}.\ \Omega_m = 0.26,\ w = -1.5,$$

as a result, the shapes of the squares appear distorted (AP effect), and their sizes are wrongly estimated (volume effect). Cosmological models (i,iii) yield to compressed size (in both angular and LOS direction), and the degree of compression increases with increasing distance; the situation is opposite for the other two cosmologies.

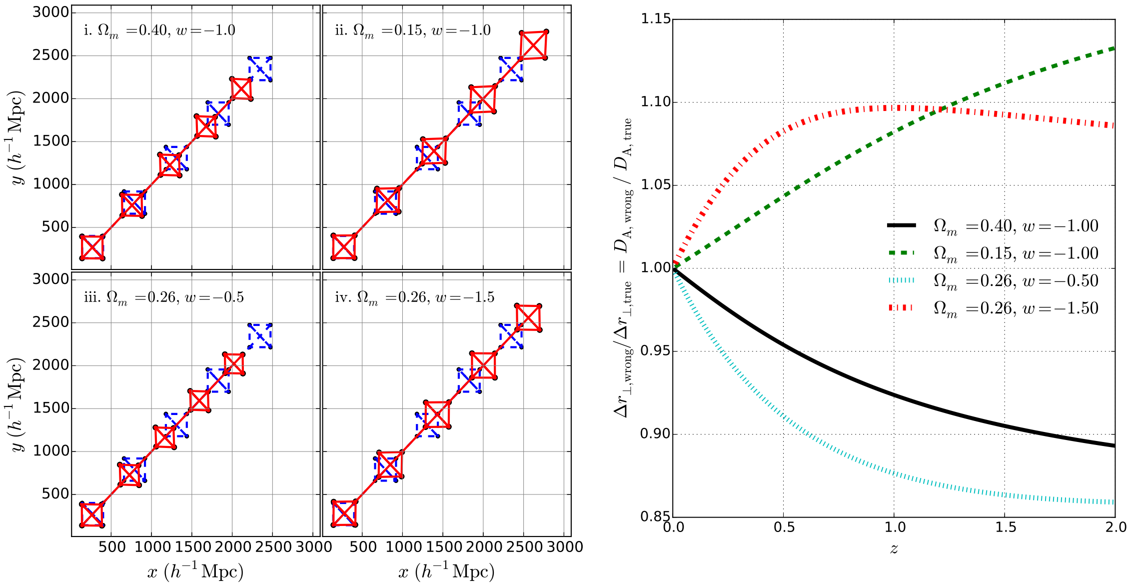


**Figure 1.** A description of how wrongly assumed cosmologies can distort the interpretation of observation, assuming $\Omega_m = 0.26, w = -1$ is the true cosmology. Left panel shows a series of five regular squares, measured by an observer at the origin. Their true positions and shapes are plotted in blue dashed lines. When the observer adopts the wrong cosmologies to compute the distance from measured redshifts and infer the positions and shapes of the squares, he/she obtains distorted squares shown as the red solid lines. Right panel shows the redshift evolution of the wrongly estimated angular diameter distance (divided by the correct value).

The mis-estimation of angular size, $\Delta r_{\perp,\mathrm{wrong}}/\Delta r_{\perp,\mathrm{true}}$, is displayed in the right panel of Figure 1. In all cosmologies, $\Delta r_{\perp,\mathrm{wrong}}/\Delta r_{\perp,\mathrm{true}}$ evolves a lot in the redshift range $0 < z < 2$. As an example, when adopting the quintessence cosmology $\Omega_m = 0.26,\ w = -0.5$, the angular size is underestimated by 8.9%, 12.3%, 13.6%, 14.1% at $z = 0.5, 1, 1.5, 2$.

In sum, as a consequence of incorrect cosmologies, the size of objects is mis-estimated, and the magnitude of mis-estimation depends on the redshift. We use the galaxy angular 2pCF to probe the mis-estimation of angular size, $\Delta r_{\perp,\mathrm{wrong}}/\Delta r_{\perp,\mathrm{true}}$.

## 3. THE SIMULATION DATA

We test the method using the mock galaxy samples produced by the Horizon Run 4 (HR4) N-body simulation (Kim et al. 2015; Hong et al. 2016).

HR4 was made within a cube of volume $(3.15\,h^{-1}\mathrm{Gpc})^3$ using $6300^3$ particles with mass $m_p \simeq 9 \times 10^9 h^{-1}\mathrm{M}_\odot$. The simulation adopted the second order Lagrangian perturbation theory (2LPT) initial conditions at $z_i = 100$ and a WMAP5 cosmology $(\Omega_b, \Omega_m, \Omega_\Lambda, h, \sigma_8, n_s) = (0.044, 0.26, 0.74, 0.72, 0.79, 0.96)$ (Komatsu et al. 2011).

Mock galaxies are produced from the simulation based on a modified one-to-one correspondence scheme (Hong et al. 2016). The most bound member particles (MBPs) of simulated halos are adopted as tracers of galaxies. The merger timescale is computed to get the lifetime of merged halos. Merger trees of halos are constructed by tracking their MBPs from $z = 12$ to 0; when a merger event occurs, the merger timescale is computed using the formular of Jiang et al. (2008) to determine when the satellite galaxy is completely disrupted.

The resulting mock galaxies was found to reproduce the 2pCF of SDSS DR7 volume-limited galaxy sample (Zehavi et al. 2011) very well. The mock galaxies shows a similar finger of god (FOG) feature (Jackson 1972) as the observation. The projected 2pCF of the mock and observational samples agree within $1\sigma$ CL on scales greater than 1 $h^{-1}$Mpc.

We take the snapshot data of the mock galaxies at $z = 0, 0.5, 1, 1.5, 2$. Setting a minimal halo mass of $3 \times 10^{11} h^{-1}\mathrm{M}_\odot$, we select 457, 406, 352, 206 and 228 million mock galaxies at the five redshifts, corresponding to a number density of 1.46, 1.30, 1.13, 0.98 and 0.73 in unit of $10^{-2} h^3\mathrm{Mpc}^{-3}$, respectively. By applying a uniform mass cut, at higher redshift we have smaller number of galaxies with *larger bias*.

As an illustration, Figure 2 displays the 2D distribution of a subsample of mock galaxies in five redshifts, with $x$, $y$ coordinates computed using the "correct" cosmological parameters $\Omega_m = 0.26,\ w = -1$ (left panels) and a set of wrong cosmological parameters $\Omega_m = 0.05,\ w = -1.5$ (right panels), respectively.

When the correct cosmology is adopted the cosmic scale is correctly estimated, the main factor leads to redshift evolution of galaxy distribution is the gravitational growth of structure. With the decreasing the redshift, we clearly see the clusters and filaments form and grow. On the other hand, when the wrong cosmology is adopted, there is an artifical scaling of scales in the constructed map. The separations among galaxies are overestimated by $25.6\%, 47.3\%, 62.2\%, 71.7\%$ at redshifts of $0.5, 1.0, 1.5, 2.5$, leading to a clear redshift evolution of sizes of structures.

The growth of structure strengths the clustering and make structures more compact, while the volume effect maintain the clustering pattern and uniformly re-scale the structures on all scales. Their imprints on the large scale structure is different and should be distinguishable. In the following, we show that they affect the angular correlation function measurements in different ways, and can be easily separated.

## 4. METHODOLOGY

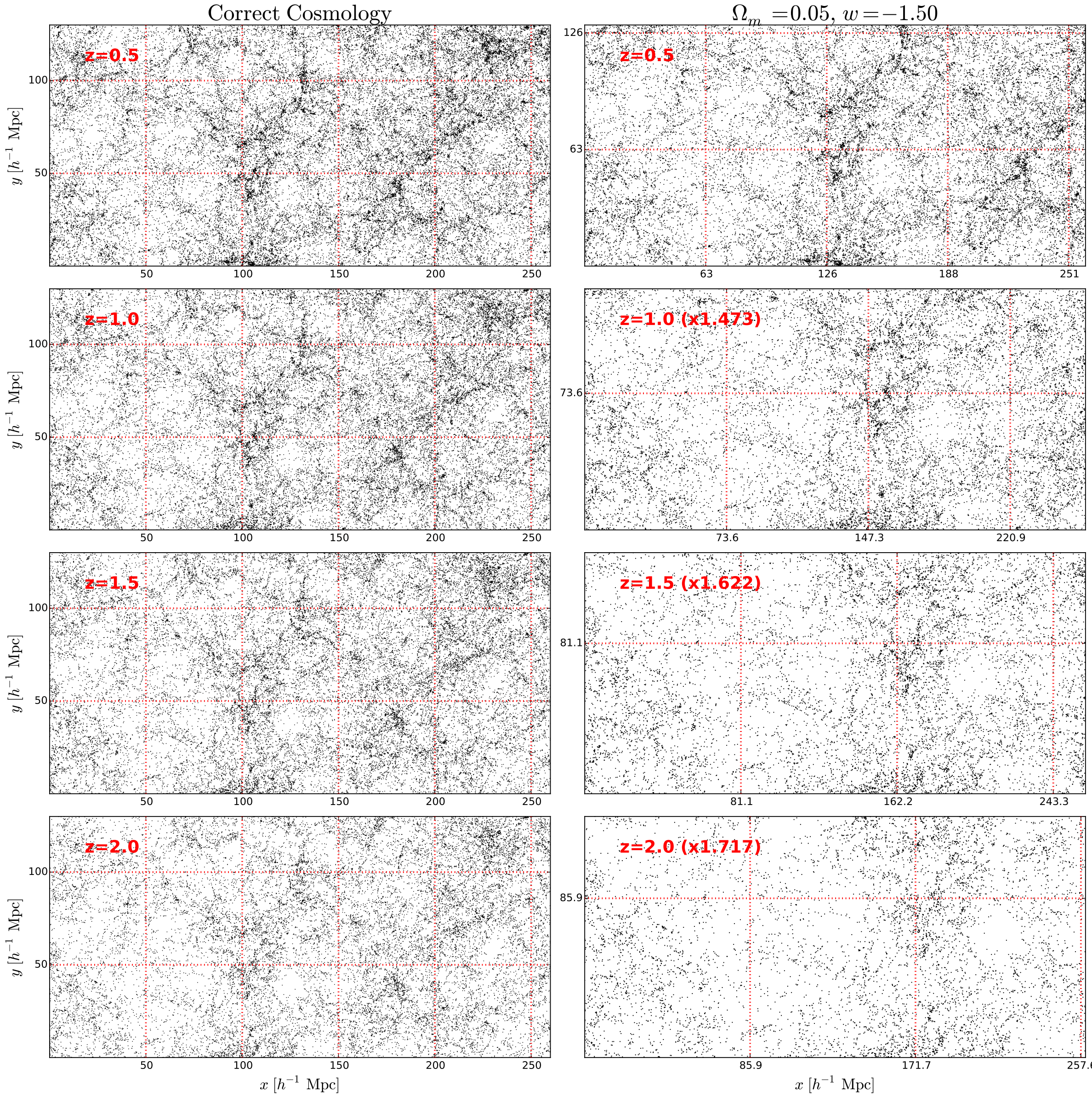


**Figure 2.** The 2D distribution of a $260\times130\times105(h^{-1}\mathrm{Mpc})^3$ subsample of HR4 mock galaxies, at redshifts 0.5, 1, 1.5 and 2. Left and right panels whos the $x$, $y$ coordinates computed using the "correct" parameters $\Omega_m = 0.26,\ w = -1$ and a set of wrong cosmological parameters $\Omega_m = 0.05,\ w = -1.5$, respectively. The growth of structure strengths the clustering and make structures more compact at lower redshift. When the wrong cosmology is adopted, the covmoving distances is mis-scaled and over-estimated by 25.6%, 47.3%, 62.2%, 71.7% at redshifts of $0.5, 1.0, 1.5, 2.5$, leading to a clear redshift evolution of sizes of structures.

We use the angular 2pCF as a statistical tool to probe the volume effect. The galaxy 2pCF as a function of galaxy separation in the angular direction, $\omega(r_\perp)$, is computed for snapshot data of mock galaxies at redshifts 0.5, 1, 1.5 and 2. We adopt the Landy-Szalay estimator (Landy & Szalay 1993),

$$\omega(r_\perp) = \frac{DD - 2DR + RR}{RR}\ , \tag{4}$$

where $DD$ is the number of galaxy–galaxy pairs, $DR$ the number of galaxy-random pairs, and $RR$ is the number of random–random pairs, all separated by a distance defined by $r_\perp \pm \Delta_{r_\perp}$ where we choose $\Delta_{r_\perp} = 1h^{-1}$Mpc. The random catalogue consists of unclustered points uniformly distributed in a same size box. In an effort to reduce the statistical variance of the estimator, we use 50 times as many random points as we have galaxies.

Considering the large number of galaxies and random points the 2pCF is computed part by part in subsamples with size of $1575\ h^{-1}\mathrm{Mpc}\times1575\ h^{-1}\mathrm{Mpc}\times105\ h^{-1}\mathrm{Mpc}$. The sheet shape of the subsample is close to the shape of redshift shells in the real observational case. The Z direction with thickness 105 $h^{-1}$Mpc is treated as the radial direction (the $r$ direction) and the X-Y directions are the angular plane. For our simulation box size we have 120 such subsamples. The average of the measurements in all subsamples is adopted as the 2pCF of the whole sample, while the covariances of them are adopted as the covariance matrix (after multiplying a factor of $1/\sqrt{119}$).

### 4.1. *Galaxy angular 2pCF: at different redshifts*

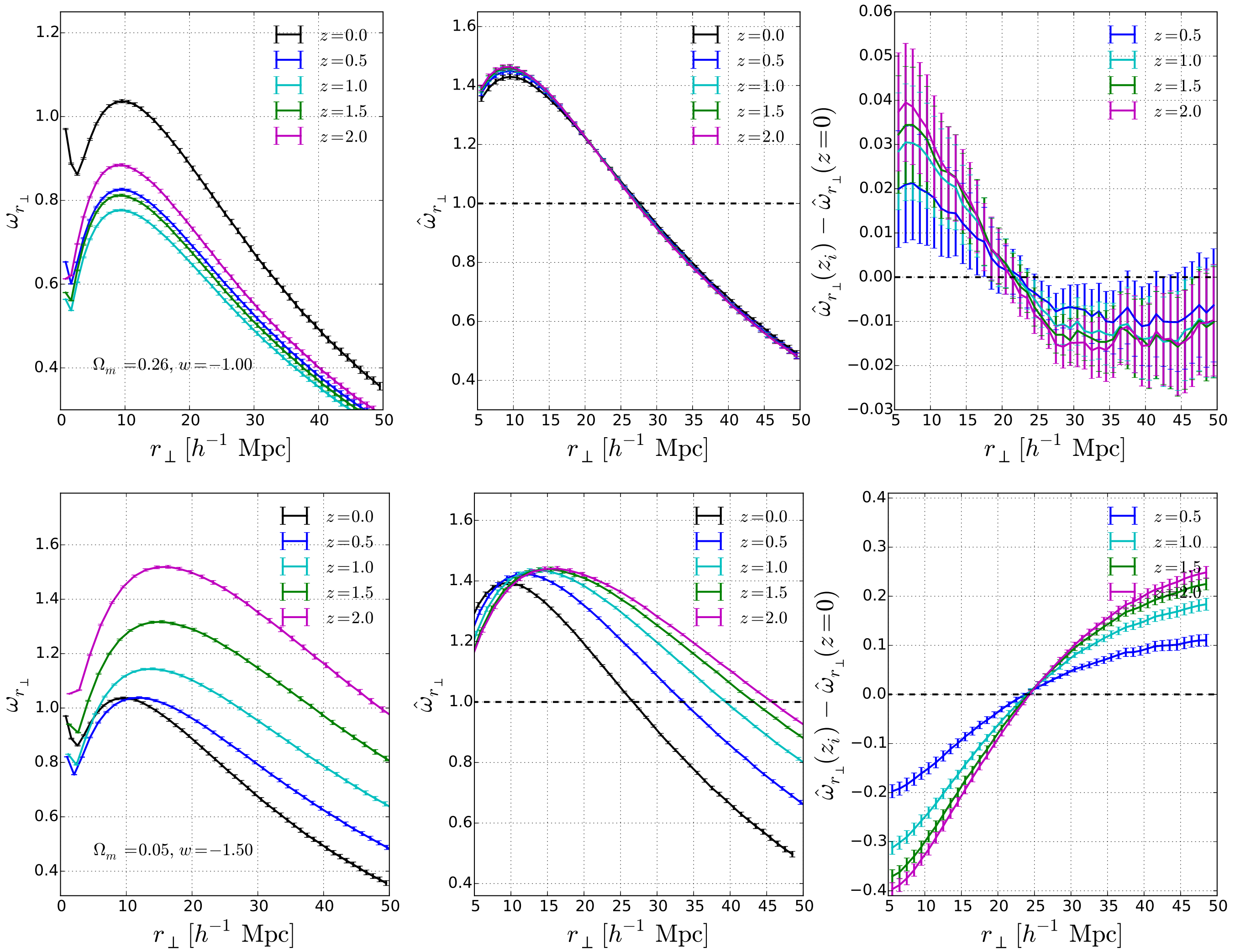


**Figure 3.** The angular 2pCF ($\omega_{r_\perp}$, left panels), the shape of the angular 2pCF ($\hat{\omega}_{r_\perp}$, middle panels), and the evolution with respect to the $z = 0$ value ($\hat{\omega}_{r_\perp}(z = z_i) - \hat{\omega}_{r_\perp}(z = 0)$, right panels). Upper panels show that in the correct cosmology the redshift evolution of the shape of 2pCF is rather small, whereas the lower panels show that, in a wrong cosmology $\Omega_m = 0.05, w = -1.5$, the redshift evolution of $\hat{\omega}_{r_\perp}$ is very significant.

The upper-left panel of Figure 3 displays the angular 2pCF measured from HR4 mock galaxies. We multiply $\omega$ by the separation $r_\perp$ to have similar size of statistical uncertainty on all scales.

Among different redshifts there is large variation in the amplitude of $\omega(r_\perp)$. The amplitude is proportional to the clustering strengh which is affected by the gravitational growth of structures and the galaxy bias. The amplitude is highest at $z = 0$ where the structures experienced most growth. $\omega(r_\perp)$ also increases with redshift at $z > 1$ with increasing redshift as a reason of increasing galaxy bias.

Different from the large variation of amplitude among different redshifts, the shape of $r_\perp\omega$ maintains similar at all redshifts; in general it peaks at $r \sim 9h^{-1}$Mpc and monotonically drops or increases at larger or smaller scales. The only exception is the small enhancement at $r \lesssim 2h^{-1}$Mpc, which is caused by the non-linear growth of structures and is much more significant at lower redshfit.

In order to directly compare the shape of 2pCF at different redshifts, in the middle panel of Figure 3 we show the $r_\perp\omega$ normalized by the overall amplitude within $5h^{-1}\mathrm{Mpc} < r < 40h^{-1}\mathrm{Mpc}$ (here after $\hat{\omega}_{r_\perp}$):

$$\hat{\omega}_{r_\perp} \equiv \frac{r_\perp \omega(r_\perp)}{\int_{r_{\perp,\mathrm{min}}}^{r_{\perp,\mathrm{max}}} r_\perp \omega(r_\perp) dr_\perp / (r_{\perp,\mathrm{max}} - r_{\perp,\mathrm{min}})}, \tag{5}$$

where we choose $r_{\perp,\mathrm{min}} = 5h^{-1}$ Mpc, $r_{\perp,\mathrm{max}} = 40h^{-1}$ Mpc in this analysis. Below $5h^{-1}$ Mpc the non-linear growth of structure leads to systematic redshift evolution which could be difficult to be reliably accounted; On scales larger than $40h^{-1}$ Mpc, the analytical modelling of the shape of the angular 2pCF is relatively well understood; one can just fit the 2pCF with the theoretical predictions (Salvador et al. 2014, 2016) instead of using our method (although out method should is also applicable).

In the upper-middle panel, the nice overlapping of the $\hat{\omega}_{r_\perp}$ more clearly shows the the small redshift evolution of the shape. In the upper-right panel, we further show the residual evolution at high redshifts with respect to $z = 0$. There is only 1-4% enhancement at $r < 10h^{-1}$Mpc, and $< 1.5\%$ suppression at $r > 25h^{-1}$Mpc. The trend is monotonic with redshift.

There is one detail in the analysis which should be emphasized here. In real observations we are observing *different* objects in different redshift shells. Considering this fact in the comparison of $\hat{\omega}_{r_\perp}$ we compare subsamples of galaxies at *different* locations. As an exammple, if at $z=0$ we take $\hat{\omega}_{r_\perp}$ measured within $0h^{-1}$Mpc $< Z < 105h^{-1}$Mpc, at higher redshifts we then adopt measurement within $105h^{-1}$Mpc $< Z < 210h^{-1}$Mpc for a comparision. If simply comparing the 2pCF of a *same* subsample of galaxies at different redshifts, one would significantly underestimate the statistical undertainty of $\delta\hat{\omega}_{r_\perp}$ by ignoring the cosmic variance.

### 4.2. *Galaxy angular 2pCF: Cosmological Effect*

The angular 2pCF of galaxy positions constructed in a wrong cosmology $\Omega_m = 0.05$, $w = -1.5$ is displayed in the lower panels of Figure 3. The mis-scaling uniformly shifts clustering patterns on all scales, leading to a wrong $\hat{\omega}_{r_\perp}$ related with the correct one as

$$\hat{\omega}_{r_\perp,\mathrm{wrong}}(r) = \hat{\omega}_{r_\perp,\mathrm{correct}}(\alpha_\perp r), \tag{6}$$

a simple consequence of the fact that clustering patterns at scale $r$ is rescaled to $\alpha_\perp r$. The redshift evolution of $\alpha_\perp$ leads to redshift evolution of $\hat{\omega}_{r_\perp,\mathrm{correct}}$, which is displayed in the lower-middle panel. The upscaling of comoving distance leads to a stretched shape. With the increasing of redshift, the peak location is shifted from $9h^{-1}$Mpc to $15h^{-1}$Mpc at $z=2$, as a result of the fact that the angular separation is upscaled by 71.7%. Correspondingly, the right panel shows that, compared with $\hat{\omega}_{r_\perp}$ at $z=0$ there is a 20-40% change at higher redshifts.

The mis-scaling not only changes the shape of the 2pCF but also modifies its amplitude. As is shown in the left panel, due to the stretch of scale the amplitude is enhanced at higher redshifts; the higher the redshift, the more the enhancement.

Although the change of amplitude could be a more significant cosmological consequence than the alteration of shape, it is mixed with the other effects; the growth of structure and a larger galaxy bias can also lead to a stronger clustering and thus an enhanced amplitude. In order to reliably extract the cosmological information, we just utilize the the redshift evolution of the 2pCF shape, which is less affected by other factors.

### 4.3. *Systematic effects*

Sec. 4.1 shows that $\hat{\omega}_{r_\perp}$ measured from constant mass cut samples at different redshifts is close to each other. The gravitational growth of structure will not have large impact on $\hat{\omega}_{r_\perp}$ on scales $\gtrsim 5h^{-1}$ Mpc. Yet there are many other factors may introduce redshift evolution, including galaxy bias, RSD, redshift error, and the redshift evolution of properties of galaxies such as the mass, morphology, color, concentration, and so on. Here we test two "major" systematical effects, the galaxy bias and the RSD effect.

#### 4.3.1. *Galaxy Bias*

Galaxies are biased tracers of dark matter field; more massive galaxies reside in regions with higher density contrast and exhibit stronger clustering (i.e. larger bias).

We vary the mass cut and check the effect of galaxy bias on $\hat{\omega}_{r_\perp}$. The upper panels of Figure 4 displays the 2pCF measured from galaxies within a $3175\times3175\times105$ $(h^{-1}\mathrm{Mpc})^3$ volume, taken from the $z=0$ snapshot. Four values of minimal mass limits, $3\times10^{11}M_\odot$, $1\times10^{12}M_\odot$, $4\times10^{12}M_\odot$ and $1\times10^{13}M_\odot$, are imposed to create three samples with different galaxy bias. The measured angular 2pCF are displayed.

The different mass cuts result in large variation in the amplitude of the 2pCF (left panel), while the shape of the 2pCF remains less affected (middle panel). Compared with the sample of $M > 3\times10^{11}M_\odot$, samples with mass limits of $1\times10^{12}M_\odot$, $4\times10^{12}M_\odot$ and $1\times10^{13}M_\odot$ have amplitude of 2pCFs enhanced by 10%, 50% and 100%, while the change in the shape is only 0.5%, 2% and 4%. The effect of galaxy bias becomes much smaller by utilizing the shape of the 2pCF rather than the amplitude.

#### 4.3.2. *Redshift Space Distortion*

The galaxy peculiar velocity contributes to the observed redshift and distorts the inferred galaxy radial position, known as the redshift space distortion. It is the major systematics in our previous works (Li et al. 2014, 2015, 2016) of statistical analysis on the 3D galaxy distribution.

The effect of RSD is much milder in this work. The angular positions of galaxies are not shifted by RSD at all; the only effect of RSD enter in the procedure of splitting galaxies into redshift shells. The galaxies observed in a survey are split into shells of subsamples, with different redshift ranges, for the 2pCF measurement. RSD distorts the galaxy redshift and as a result some galaxies (especially those close to the boundaries of shells) are classified to wrong redshift shells.

The lower panel of Figure 4 displays the RSD effect on 2pCF. We shift the radial coordinates of galaxies according to the relation

$$\Delta z = (1+z)\frac{v_{\mathrm{Z}}}{c}, \tag{7}$$

where $v_{\mathrm{Z}}$ (Z is treated as the radial direction in this analysis) is the galaxy peculiar velocity in the LOS direction. This lead to mis-classification of some galaxies when we split the box into slices.

Comparing the plot with Figure 3 one clearly see the effect of RSD. The amplitude of measured 2pCF is enhanced by $\sim 10\%$ in case of considering the RSD effect. The slop of $\hat{\omega}_{r_\perp}$ slightly suppressed. While the redshift evolution of $\hat{\omega}_{r_\perp}$ is still small... Although the pattern is a little modified... So RSD is not a big issue here... **after anna jobs finished we have better plots and re-revise this section**

Similar to RSD, redshift errors of galaxies also results in fuzzy boundaries of shells and mis-classification of galaxies. This effect should also be properly quantified in real observations.

### 4.4. *Likelihood Analysis*

A cosmology resulting in smaller evolution is considered to be more likely to be the correct one. The procedure here is very similar to what we did in Li et al. (2014, 2015, 2016). We compare the high redshift $\hat{\omega}_{r_\perp}$ and the lowest redshift measurement,

$$\delta r\hat{_\perp}\omega(z_i,z_1) \equiv r\hat{_\perp}\omega(z_i) - r\hat{_\perp}\omega(z_1), \tag{8}$$

and design the likelihood function to quantify the redshift evolution of $\hat{\omega}_{r_\perp}$:

$$\chi^2 \equiv \sum_{i=2}^{n_z}\sum_{j_1=1}^{n_r}\sum_{j_2=1}^{n_r} \mathbf{p}(z_i,r_{j_1})(\mathbf{Cov}_i^{-1})_{j_1,j_2}\mathbf{p}(z_i,r_{j_2}), \tag{9}$$

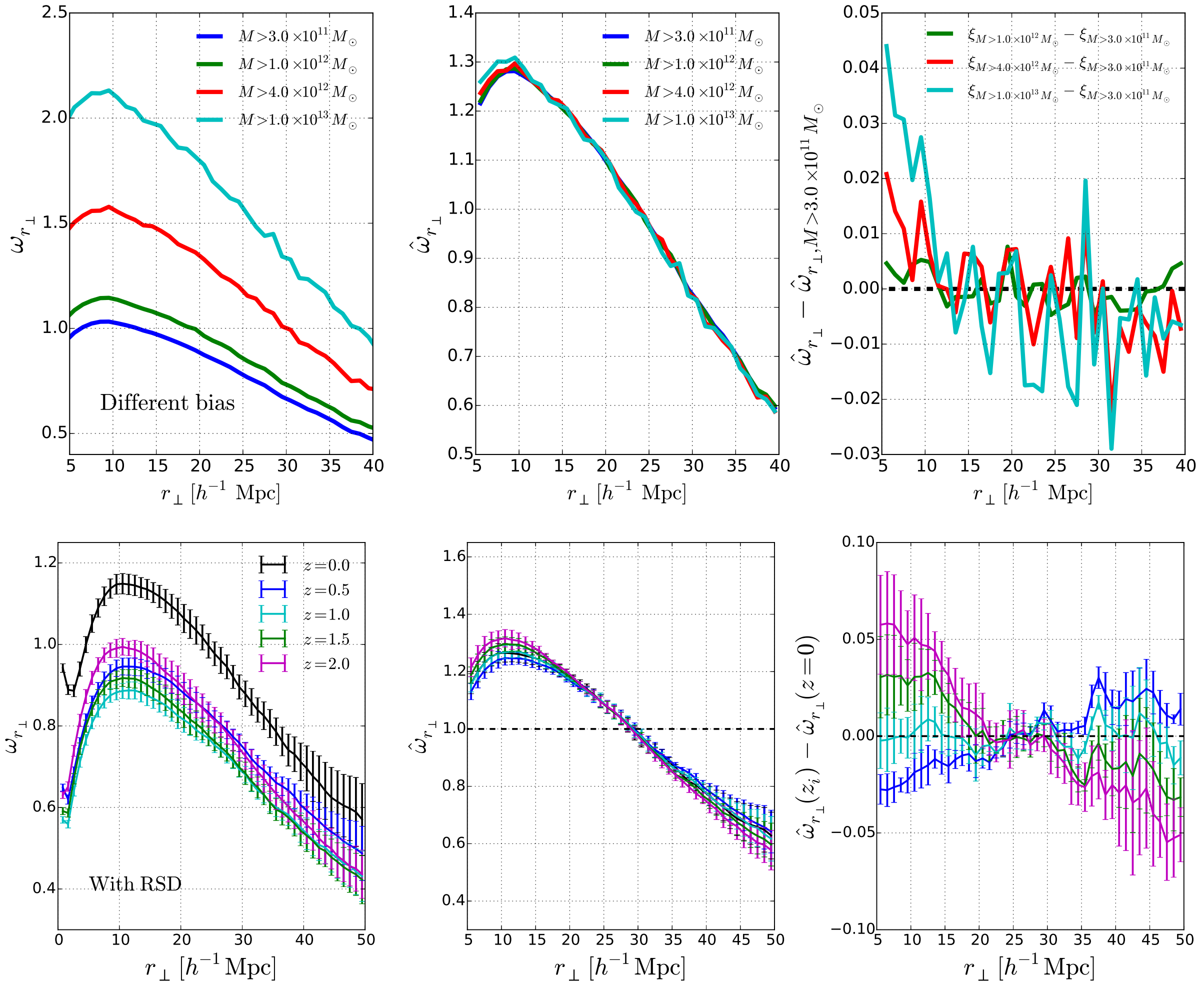


**Figure 4.** Upper panels: $\omega_{r_\perp}$ (left) and $\hat{\omega}_{r_\perp}$ (middle) are shown for four different halo-mass-cuts, $3\times10^{11}$, $1\times10^{12}$, $4\times10^{12}$, & $1\times10^{13}$ $M_\odot$, below which we remove from 2pCF calculation. The right panel shows the difference in $\hat{\omega}_{r_\perp}$ between the $3\times10^{11}$ $M_\odot$ mass-cut case and the other mass-cut cases. Lower panels: $\omega_{r_\perp}$ (left), $\hat{\omega}_{r_\perp}$ (middle), and $\hat{\omega}_{r_\perp}(z=z_i)-\hat{\omega}_{r_\perp}(z=0)$ (right) calculated with the RSD effect included.

where $n_z$ is the number of redshifts which is 5 in this analysis, $n_r$ is number of binning in $\hat{\omega}_{r_\perp}(r_\perp)$, which is 35 since we have $r_\perp$ bins with width $1h^{-1}$Mpc in a range of $5h^{-1}\text{Mpc}\le r\le 40h^{-1}\text{Mpc}$. $\mathbf{p}(z_i,r_j)$ is the redshift evolution of the angular correlation function shape with systematic effects subtracted

$$\mathbf{p}(z_i,r_j)\equiv\ \delta\hat{\omega}(z_i,z_1,r_j)-\delta\hat{\omega}_{r_\perp,\mathrm{sys}}(z_i,z_1,r_j) \quad (10)$$

$\mathbf{Cov}_i$ is the covariance matrix estimated from the $\mathbf{p}(z_i,r_j)$ measured from 120 subsamples. As mentioned before, for a robust estimation of covariance matrix, we always compare slices at different locations to include the cosmic variance.

The covariance matrix inferred from a finite number of samples is always a biased estimate of the true matrix (Hartlap et al. 2006). This can be corrected by rescaling the inverse covariance matrix as

$$\mathbf{Cov}^{-1}_{ij,\mathrm{Hartlap}}=\frac{N_s-n_r-2}{N_s-1}\mathbf{Cov}^{-1}_{ij}, \quad (11)$$

where $N_s=120$ is the number of mocks used in covariance estimation. For this analysis the rescaling is as large as 1.43. In the case that one have 2 000 mocks the rescaling is less than 1.02.

Figure 5 displays the 2pCF and the likelihood values in case of adopting the four wrong cosmologies of Figure 1. For the cosmologies $\Omega_m=0.4,w=-1$ and $\Omega_m=0.26,w=-0.5$, the compression shifts the large scale clustering patterns into small scales at higher redshift and make the 2pCFs steeper. For cosmologies $\Omega_m=0.15,w=-1$ and $\Omega_m=0.26,w=-1.5$, the stretch of structure leads to shallower slope of $\hat{\omega}_{r_\perp}$ at higher redshift. In all cosmologies there is significant detection of redshift evolution. We compute the $\chi^2$ values according to Equation 9, and find these cosmologies are disfavored at $\gtrsim 30\sigma$ CL.

## 5. COSMOLOGICAL CONSTRAINT

We constrain $\Omega_m$ and $w$ through Bayesian analysis (Christensen et al. (2001); also see Lewis & Bridle (2002); Li et al. (2016)). We assue the likelihood takes the form

$$\mathcal{L}\propto\exp\left[-\frac{\chi^2}{2}\right], \quad (12)$$

and scan the parameter space in $\Omega_m-w$ plane to obtain the 68.3% and 97.4% CL regions. The result is displayed in Figure 6.

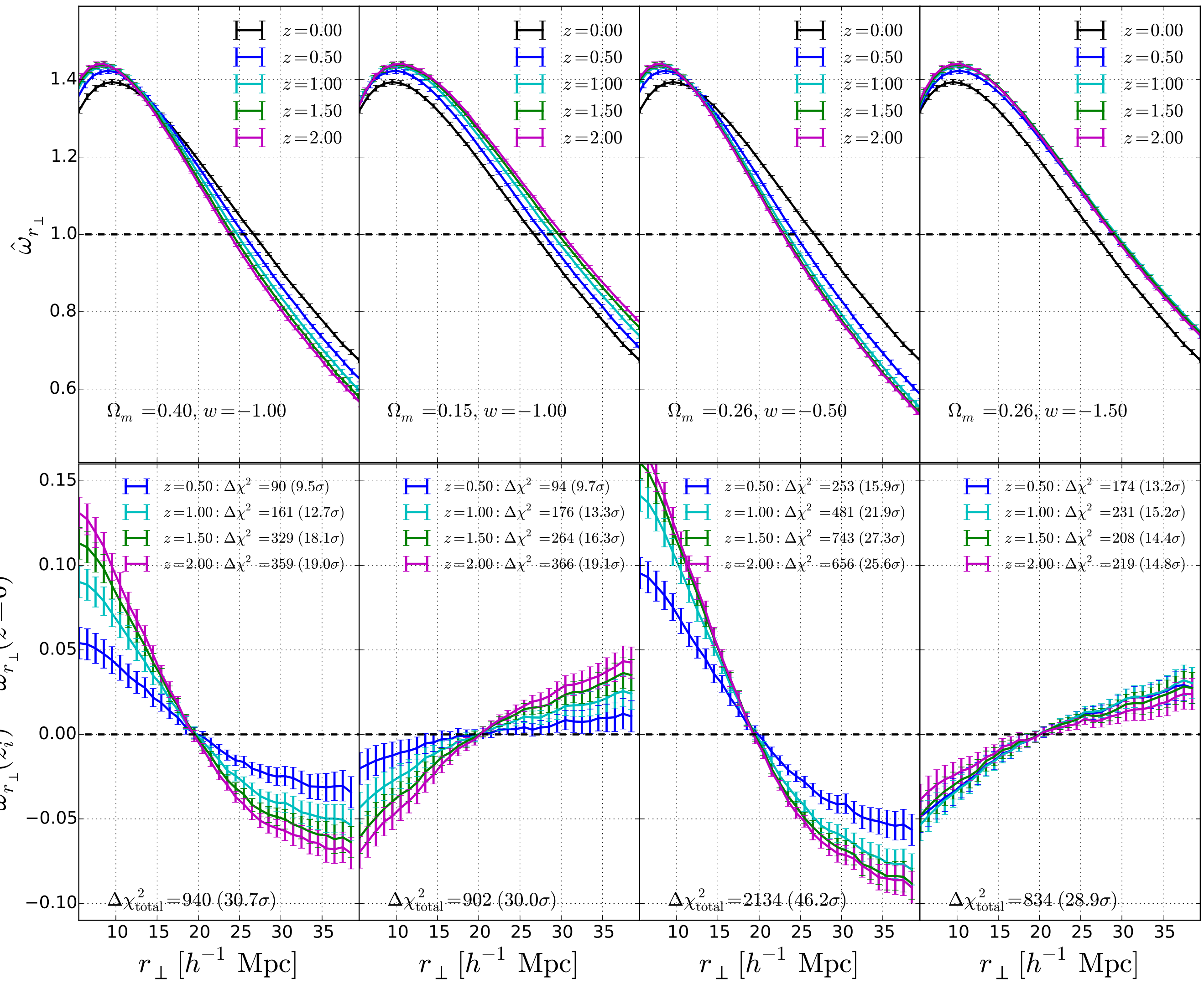


**Figure 5.** $\hat{\omega}_{r_\perp}$ (upper panels) and $\hat{\omega}_{r_\perp}(z=z_i) - \hat{\omega}_{r_\perp}(z=0)$ (lower panels) at several redshifts, for the four wrong cosmologies. The redshift evolution of angular 2pCF shape in these wrong cosmologlies are detected at high CL.

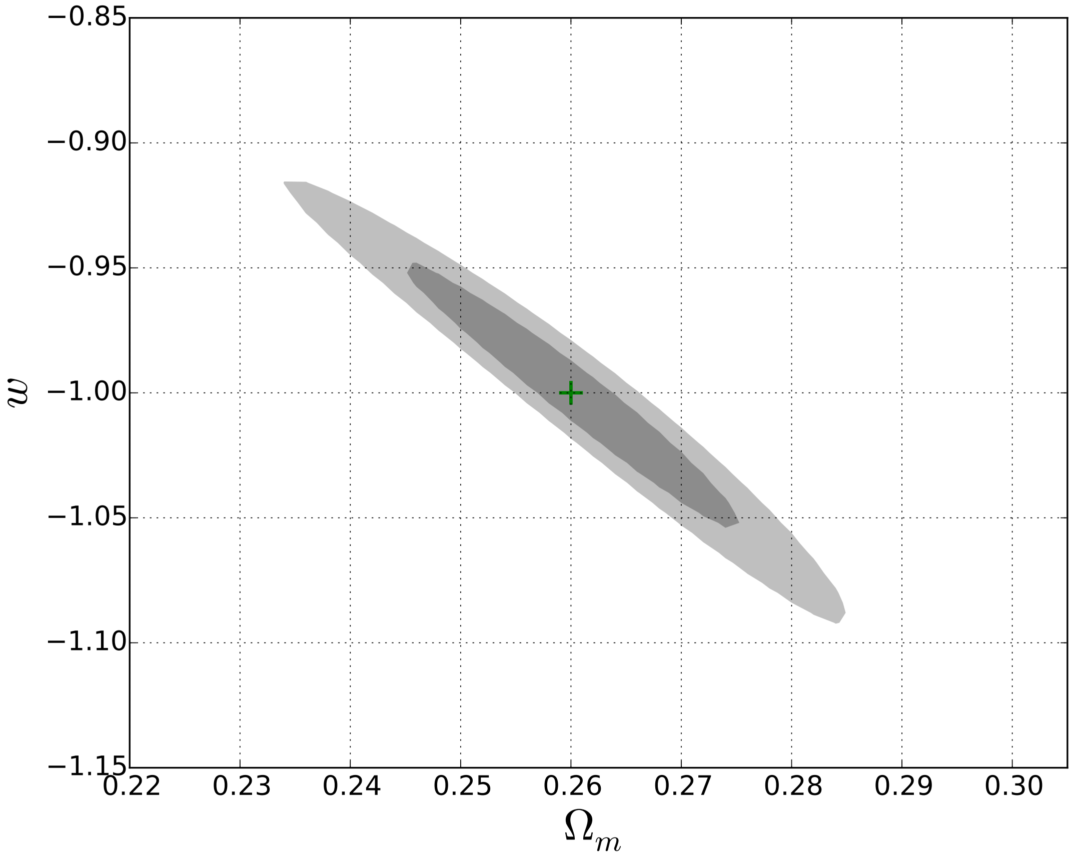


**Figure 6.** Likelihood contours (68.3%, 95.4%) in the $\Omega_m - w$ plane from our method, a likelihood value computed using Equations (**??**), based on the redshfit evolution of the angular 2pCF shape $\hat{\omega}_{r_\perp}$. Utilizing the HR4 snapshots data of mock galaxies at five redshifts, the method can lead to very tight cosmological constraint.

We get tight constraint on the two paramters. The $2\sigma$ contour lies within the region $0.23 < \Omega_m < 0.285$, $-1.1 < w < -0.9$. The two parameters are very strongly degenerated with each other. The thin shape of contour implies that, when combining with the another observational data with different direction of degeneracy (e.g. CMB, BAO), very tight combined constraint can be obtained. In case of fixing one parameter at its best-fit value and constrain the other one, one obtain $1\sigma$ uncertainty of $\delta\Omega_m \approx 0.002, \delta w \approx 0.01$.

## 6. CONCLUDING REMARKS

We developed a method measuring the redshift of the shape of galaxy angular correlation function, $\hat{\omega}_{r_\perp}$, to constrain cosmology. A wrongly adopted cosmology result in redshift-dependent mis-scaling in the constructed galaxy distribution, which leads to redshift-dependent rescaling of $\hat{\omega}_{r_\perp}(r_\perp)$. The signal is sensitive to cosmology and relatively insensitive to the gravitational growth of structure, the galaxy bias, and the RSD effect. We test our method on the HR4 mock galaxies having 457, 406, 352, 206 and 228 million galaxies at redshfits 0, 0.5, 1, 1.5, 2. Analyzing the redshift evolution of $\hat{\omega}_{r_\perp}(r_\perp)$ on scales $5h^{-1}\mathrm{Mpc} \leq r_\perp \leq 40h^{-1}\mathrm{Mpc}$, we derive tight constraints on $\Omega_m$ and $w$.

In this analysis we restrict our focus to the rescaling in angular direction. One can also use the 2D 2pCF $\xi(s,\mu)$ as a function of both angular and radial scale to fully probe the scaling effect in 3D galaxy distribution.

There are already works using the angular 2pCF to constrain cosmology by directly comparing the theoretical 2pCF and the observed one (Salvador et al. 2014, 2016). Our method is simpler and just utilizes the fact in the correct cosmology the angular 2pCF shape does not exhibit much redshift evolution. Our method is complementary to these works in that it does not require accurate analytic modeling, and could be applicable on smaller scales.

Li et al. (2015, 2016) shows that using the redshift dependent of AP effect one can derive very tight cosmological constraint. These two methods probe different information encoded in the 2pCF and can be combined to have a complete geometric probe of LSS galaxy distribution.

This method is designed to be applied to current and future LSS surveys, with a particular emphasis to the *photometric surveys*, such as DES (300 million galaxies at $z \lesssim 1.5$) and LSST (20 billion galaxies at $z \lesssim 2$) [CHECK THEM!!!]. These surveys probe a large amount of galaxies and the redshift error will not quite affect the angular 2pCF measurement as long as the redshift dependence of the photometric redshift can be reliably understood.

Our series of works Li et al. (2014, 2015, 2016), together with this analysis, and also (Park & Kim 2010; Morandi & Sun 2016), are introducing a new strategy to constrain cosmology from LSS data. We seek for the statistical pattern which maintains nearly constant at all redshifts; this invariance is broken if wrong cosmologies are adopted to construct the galaxy distribution and introduces redshift evolution of geometric distortion. The systematic effects can be corrected by performing a N-body simulation in a cosmology with values of parameters close enough to the underlying correct one. This avoids the difficult modeling of galaxy bias, galaxy clustering and RSD, enables reliable cosmological constraint on scales much smaller than BAO. We hope these methods play an important role in deriving cosmological constraints from future LSS surveys.

## ACKNOWLEDGMENTS

We thank the Korea Institute for Advanced Study for providing computing resources (KIAS Center for Advanced Computation Linux Cluster System). We would like to thank Stephen Appleby and Yi Zheng for kind helps and valuable comments. This work was partially supported by the Supercomputing Center/Korea Institute of Science and Technology Information with supercomputing resources including technical support (KSC-2013-G2-003).

## APPENDIX

## REFERENCES

Alam, S., Ata, M., & Bailey, S., et al. 2016, submitted to MNRAS (arXiv:1607.03155)
Alcock, C., & Paczynski, B. 1979, Nature, 281, 358
Ballinger, W.E., Peacock, J.A., & Heavens, A.F. 1996, MNRAS, 282, 877
Beutler, F., Blake, C., & Colless, M., et al. 2011, MNRAS, 416, 3017
Beutler, F., Saito, S., & Seo, H.-J., et al. 2013, MNRAS, 443, 1065
Beutler, F., Seo, H.-J., & Saito, S., et al. 2016, arXiv:1607.03150
; Blake, C., & Glazebrook, K. 2003, ApJ, 594, 665
Blake, C., Glazebrook, K., & Davis, T. M., 2011, MNRAS, 418, 1725
Christensen, N., Meyer, R., Knox, L., & Luey, B. 2001, Class. Quant. Grav., 18, 2677
Chuang, C.-H., & Wang, Y. 2012, MNRAS, 426, 226
Eisenstein, D.J., Hu, W., & Tegmark, M. 1998, ApJ, 504, L57
Hartlap J., Simon P. & Schneider P. [astro-ph/0608064].
Hong, S.E., Park, C.,& Kim, J. 2016, ApJ, 823, 103
Jackson, J., 1972, MNRAS, 156, 1
Jennings, E., Baugh, C.M., & Pascoli, S. 2011, MNRAS, 420, 1079
Jeong, D., Dai, L., Kamionkowski, M., & Szalay, A.S. 2014, arXiv:1408.4648
Jiang, C.Y., Jing, Y. P., & Faltenbacher, A., et al. 2008, ApJ, 675, 1095
Kaiser, N. 1987, MNRAS, 227, 1
Kim, J., Park, C., L'Huillier, B., & Hong, S. E. 2015, JKAS, 48, 213
Kim, J., Park, C., Rossi, G., Lee, S.M., & Gott, J.R. 2011, JKAS, 44, 217
Komatsu, E., Smith, K. M., & Dunkley, J., et al. 2011, ApJS, 192, 18
Landy, S.D., & Szalay, A.S. 1993, ApJ, 412, 64
Lavaux, G., & Wandelt, B.D. 2012, ApJ, 754, 109
Lewis, A., & Bridle, S. 2002, Phys. Rev. D, 66, 103511
Li, M., Li, X.-D., Wang, S., & Wang, Y. 2011, Commun. Theor. Phys., 56, 525
Li, X.-D., Park, C., Forero-Romero, J., & Kim, J. 2014, ApJ, 796, 137
Li, X.-D., Park, C., Sabiu, C.G., & Kim, J. 2015, MNRAS, 450, 807
Li, X.-D., Park, C., Sabiu, C.G., & Kim, J. 2016, submitted to ApJ
Linder, E.V., Minji, O., Okumura, T., Sabiu, C.G., & Song, Y.-S. 2014, Phys. Rev. D, 89, 063525
López-Corredoira, M. 2014, ApJ, 781, 96
Mao, Q., Berlind, A.A., Scherrer, R.J., et al. 2016, submitted to ApJ
Marinoni, C., & Buzzi, A. 2010, Nature, 468, 539
Matsubara T., & Suto, Y. 1996, ApJ, 470, L1
Morandi, A., & Sun, M. arXiv:1601.03741

Outram, P.J., Shanks, T., Boyle, B.J., Croom, S.M., Hoyle, F., Loaring, N.S., Miller, L., & Smith, R.J. 2004, MNRAS, 348, 745
Parejko J.K., et al., 2013, MNRAS, 429, 98
Park, C., & Kim, Y.-R. 2010, ApJL, 715, L185
Perlmutter, S., Aldering, G., & Goldhaber, G., et al. 1999, ApJ, 517, 565
Press, W.H., & Schechter, P.L. 1974, ApJ, 187, 425
Reid, B., Samushia, L., & White, M., et al. 2012, MNRAS, 426, 2719
Riess, A.G., Filippenko, A.V., & Challis, P., et al. 1998, AJ, 116, 1009
Ryden, B.S. 1995, ApJ, 452, 25
Sutter, P.M., Pisani, A., Wandelt, B.D., & Weinberg, D.H. 2014, MNRAS, 443, 2983
Salvador, S.A., Sánchez, A.G., Padilla, N.D., & Baugh, C.M. 2014, MNRAS, 443, 2612
Salvador, S.A., Sánchez, A.G., & Grieb, J.N., et al. 2016, submitted to MNRAS
Sáchez, A.G., Baugh, C.M., & Percival, W.J. et al. 2006, MNRAS, 366, 187
Sánchez, A. G., Crocce, M., Cabré, A., Baugh, C.M., & Gaztaaga, E. 2009, MNRAS, 400, 1643
Sánchez, A. G., Scoccimarro, R., & Crocce, M., et al. arXiv:1607.03147
Seo, H.-J., & Eisenstein, D.J. 2003, ApJ, 598, 720
Song, Y.S., Sabiu, C.G., Okumura, T., Oh, M., & Linder, E.V. 2014, JCAP, 12, 005
Viana, P.T.P., & Liddle, A.R. 1996, MNRAS, 281, 323
Weinberg, S. 1989, Reviews of Modern Physics, 61, 1
Weinberg, D.H, Mortonson, M.J., Eisenstein, D.J., et al. 2013, Physics Reports, 530, 87
Zehavi, I., Zheng, Z., & Weinberg, D.H., et al. 2011, ApJ, 736, 59